ChemPubSoc Europe
DOI: 10.1002/cctc.201600793
CHEMCATCHEM Full Papers

Sorption-Enhanced Steam Reforming of Glycerol over Ni–hydrotalcite: Effect of Promotion with Pt

Karan D. Dewoolkar and Prakash D. Vaidya*[a]

Sorption-enhanced steam reforming of glycerol (SESRG) is a promising method for the sustainable production of hydrogen (H_2). In this work, composites of Ni and cationic-modified hydrotalcite (HTlc) were promoted with Pt, thus resulting in two novel hybrid materials Pt-NiMgHTlc and Pt-NiCuHTlc. Activity trials for SESRG were performed in a fixed-bed reactor in the range 673–873 K and it was found that the promotion with Pt improved H_2 purity and multi-cycle durability. The best results were achieved when Pt-NiCuHTlc was employed at $T=823$ K: a H_2 concentration of 98.7 mol % and adsorption capacity of 1.34 mol CO_2/kg sorbent was achieved. When the multi-cycle performance was tested for 20 cycles, it was found that NiMgHTlc, NiCuHTlc, Pt-NiMgHTlc, and Pt-NiCuHTlc were stable for 5, 8, 13, and 18 cycles. Finally, a likely reaction pathway for SESRG over the investigated multifunctional materials was proposed.

Introduction

Hydrogen (H_2)—a clean energy carrier—can be used in fuel cells for efficient electricity production. Its carbon-neutral production from steam reforming of renewable resources such as glycerol has been extensively studied.[1,2] In particular, catalysts based on transition metals and noble metals are widely reported.[3–8] However, the steam reforming process is energy-consuming and makes many unwanted byproducts. H_2 productivity can be improved by sorption-enhanced steam reforming (SESR), which combines the reforming process with the adsorptive separation of byproduct CO_2 in a single step.

In SESR, pure H_2 is produced at low temperature by using mixtures of catalyst and chemisorbent. Thus, less energy is consumed and catalyst sintering is lowered. Also, reactors made of expensive materials are avoided. The chemisorbent captures byproduct CO_2 so that the water–gas shift (WGS) is favored, H_2 selectivity is enhanced, and subsequent processing for CO_2 separation is precluded. The adsorbent is periodically regenerated and reused. The process is cheap, simple, efficient, and widely applicable.

Notably, SESR can be applied for H_2 production from glycerol.[9–11] So far, many aspects of sorption-enhanced steam reforming of glycerol (SESRG) such as thermodynamics,[12–14] sorption kinetics,[15] and reactors[16] have been analyzed. In addition, several experimental investigations using catalyst–sorbent mixtures[17–23] (e.g., Ni or Co–Ni catalysts mixed with Ca- or Li-containing sorbents) and bifunctional catalytic materials[24,25] have also been reported. Bifunctional materials, which merge the catalytic and sorption features, are advantageous because they offer process simplicity, improved performance, and no diffusion limitations.

As seen in our previous works on SESR of methane[26] and ethanol,[27] bifunctional Ni catalysts derived from hydrotalcite-like materials are stable and active and improve H_2 production. The high reforming activity of Ni, low cost, and ease of availability are renowned.[28] Hydrotalcite-like (HTlc) basic materials, also known as layered double hydroxides, are good candidates for CO_2 sorption. Their general structure is given by $[M_{(1-x)}{}^{2+} M_x{}^{3+}(OH)_2]^{x+}\ (A^{n-})_{x/n}\cdot m\,H_2O$, where $M^{2+}=Mg^{2+}$, Mn^{2+}, Fe^{2+}, Cu^{2+}, Zn^{2+}, or Ca^{2+}, $M^{3+}=Al^{3+}$, Fe^{3+}, or Ga^{3+} and $A^{n-}=[CO_3]^{2-}$ or Cl^-.[29] They can be easily regenerated[30] and appropriately modified by the substitution of cations and anions. For example, the presence of Cu in the HTlc structure is beneficial because it promotes WGS and reduces carbon deposition,[31,32] and it is not uncommon to employ such cationic-modified hybrid materials for the SESR process.[27,33–35]

In this work, we applied basic composites of Ni and cationic-modified (Mg and Cu) hydrotalcite (HTlc), that is, NiMgHTlc (or HM1) and NiCuHTlc (or HM2) for SESRG. In addition, we promoted such composites with Pt to yield two new materials, Pt-NiMgHTlc (or Pt-HM1) and Pt-NiCuHTlc (or Pt-HM2). For the first time, we employed these novel Pt-based materials for SESRG. Pt is a popular steam reforming catalyst.[1,4,28,36] Its high activity for C–C cleavage is well-known.[1,34] Here, the influence of Pt promotion on the H_2 purity, adsorption capacity, and multi-cycle durability of the investigated composites was investigated in a fixed-bed reactor over a wide range of process conditions. So far, there is only scarce information on HTlc-based hybrid materials promoted with noble metals.[28,37–39]

---

[a] K. D. Dewoolkar, Dr. P. D. Vaidya
Department of Chemical Engineering
Institute of Chemical Technology
Nathalal Parekh Marg
Matunga, Mumbai 400019 (India)
E-mail: pd.vaidya@ictmumbai.edu.in

Results and Discussion

Characterization of hybrid materials

All the characterization details for HM1 and HM2 are reported in our previous work.[27] X-ray diffraction (XRD) profiles of the Pt-promoted hybrid materials (Pt-HM1 and Pt-HM2) before reduction are shown in Figure 1. The presence of NiO in both the hybrid materials is evident from the characteristic peaks at $2\theta = 43.4°$ and 62.8° for Pt-HM1 and $2\theta = 37.5°$ and 43.5° for Pt-HM2. A typical peak representing the presence of HTlc is seen at $2\theta = 37.3°$ for Pt-HM1. The presence of $CuAl_2O_4$ as a spinel phase was detected at $2\theta = 58.6°$ and 63°. CuO was detected at $2\theta = 39.1°$ and 49.3°. Apart from these peaks, Pt-HM2 also showed the presence of Al_2O_3, thus certifying that Al remains in its mixed oxide phase. Both these hybrid materials showed diffraction lines associated with platinum oxide at $2\theta = 75.3°$ and 75.4°, thereby suggesting the effective dispersion of Pt on the surface of the materials. The diffraction patterns observed for Pt-HM1 and Pt-HM2 were similar to those for HM1 and HM2 obtained in our previous work.[27] These results are also in good agreement with other works.[40,41] The crystallite sizes of the several phases detected from the diffraction data were calculated from the Debye–Scherrer equation. The phases and crystallite sizes of the various peaks are presented in Table 1. The surface areas of the hybrid materials, which influences activity and sorption capacity, are presented in Table 2. Both Pt-HM1 and Pt-HM2 displayed higher surface areas than HM1 and HM2. Also, the surface area of Pt-HM2 was much higher than that reported in a previous work.[40] The pore volume and pore diameter of the unused and used hybrid materials are also shown in Table 2.

Table 1. Crystallite sizes and phases of hybrid materials.

Hybrid material	Phase	2θ position [°]	Crystallite size (d) [nm]
Pt-HM1	NiO	43.4	10.4
		62.8	8.9
	Pt_2O	75.3	6.6
	HTlc	37.3	13.52
Pt-HM2	NiO	37.5	32.4
		43.5	30.8
	Pt_2O	75.4	15.7
	Al_2O_3	30.5	30.6
		35.9	32.4
		68.4	25.2
	CuO	39.1	28.3
		49.3	24.6
	$CuAl_2O_4$	58.6	20.9
		63	22

Scanning electron microscope (SEM) images of fresh Pt-HM1 and Pt-HM2 are shown in Figure 2 a, b. A highly porous and

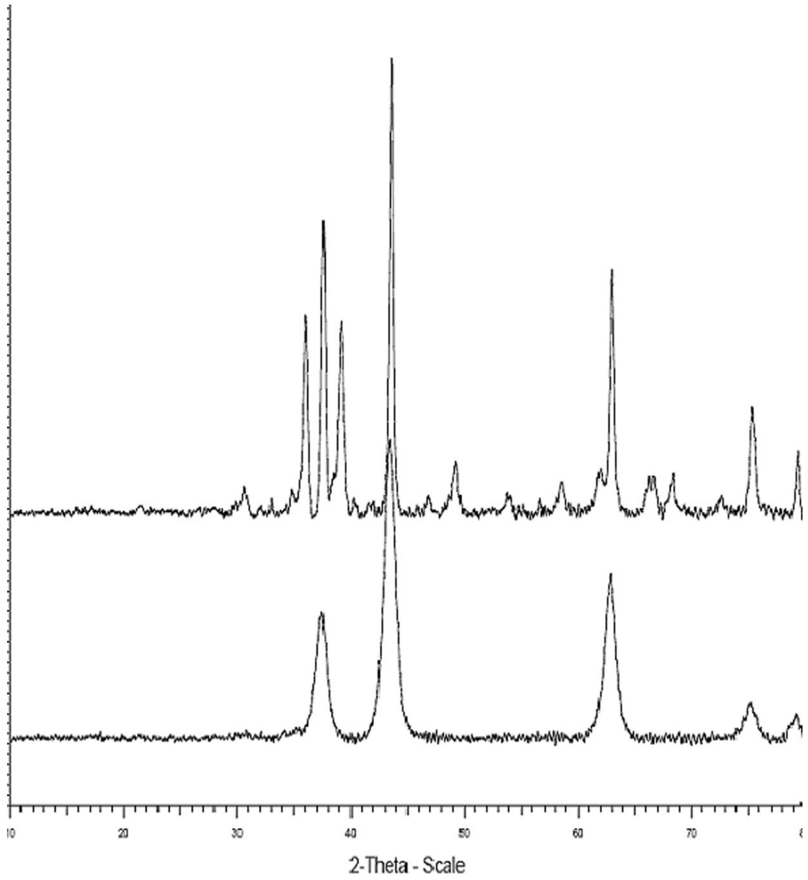

Figure 1. XRD patterns for the hybrid materials. Top pattern: Pt-HM2, bottom pattern: Pt-HM1.

Table 2. Surface area, pore volume, and pore diameter of the fresh and used (after 20 cycles) hybrid materials.

Hybrid material	Surface area [$m^2 g^{-1}$]		Pore volume [$cm^3 g^{-1}$]		Pore diameter [nm]	
	Fresh	Used	Fresh	Used	Fresh	Used
HM1	75.4	43.8	0.2	0.17	13.6	14
Pt-HM1	96.5	79.5	0.32	0.29	15.9	16.8
HM2	102	70.3	0.4	0.37	18.4	19.2
Pt-HM2	134.3	114.4	0.57	0.55	19.7	21.2

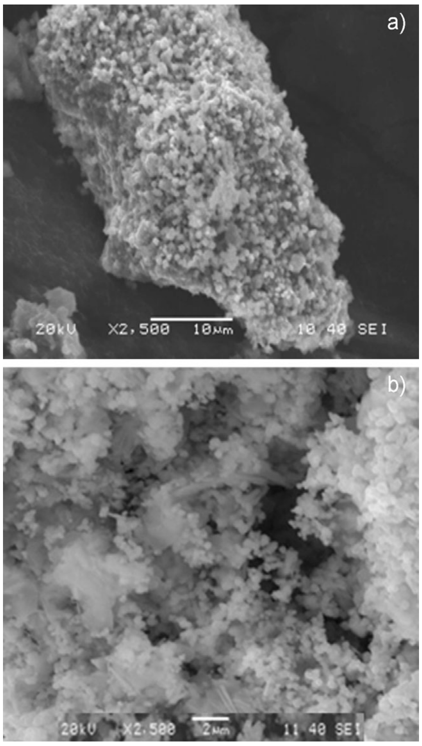

Figure 2. SEM images of hybrid materials: a) Pt-HM1, b) Pt-HM2.

granular structure was observed. The large size of the particles and their aggregation is evident. These results are in line with previous work.[34]

The chemical composition of the respective cations and anions in the hybrid materials was found by using energy dispersive X-ray spectroscopy (EDX) analysis. The ratio of Mg (63.5 mass%) to Al (23.8 mass%) in Pt-HM1 and Cu (65.3 mass%) to Al (22.4 mass%) in Pt-HM2 was about 3. The Ni content in all the samples was approximately 10 mass%.

Catalytic activity of the hybrid materials

The catalytic activity of HM1 and HM2 for glycerol conversion was investigated in the range 673–873 K. The results are presented in Figure 3. Both materials facilitated glycerol reforming. As expected, the increase in temperature resulted in increased glycerol conversion. At $T=873$ K, conversion was maximized (85.4 and 93.3% for HM1 and HM2). The higher efficacy of HM2 was attributed to the additional presence of Cu. Notably, the conversions reported in our work were higher than those reported earlier.[33,34]

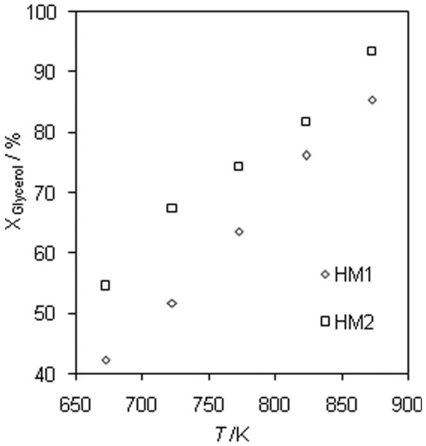

Figure 3. Glycerol conversion versus temperature plots for HM1 and HM2. Reaction conditions: $P=0.1$ MPa, GHSV $=3600$ mL $g^{-1} h^{-1}$, time on stream $=3$ h.

The influence of temperature on the gas-phase product distribution was studied and the results at a steady state in the 673–873 K range are shown in Figure 4. Similar to the results of previous works at $T>673$ K,[7,23,42,43] four major products were formed in the gas phase: H_2, CH_4, CO_2, and CO. With the rise in temperature, the H_2 concentration increased whereas the CH_4 and CO_2 content in the product decreased (see Figure 4a, b). This is possibly due to the predominance of CH_4 reforming[44] and reverse water–gas shift (RWGS)[20] at higher temperatures. Interestingly, both Pt-promoted hybrid materials displayed improved H_2 production compared with the un-promoted materials (see Figure 4c, d), owing to the high reforming and WGS activity of Pt. The merger of Pt, Ni, and Cu in a single hybrid material (Pt-HM2) favored the WGS and steam methane reforming, thereby resulting in the maximum concentration of H_2 (93.3 mole%).

At $T=873$ K, H_2 was formed in lower amounts, whereas the CO formation increased. Such behavior can be ascribed to the dominance of the RWGS reaction at high temperature.[20] No carbon deposition was observed under the tested conditions, owing to the high steam/carbon (S/C) ratios used. Also, the presence of Cu and Mg induces an electronic effect on the active phase of Ni, thereby avoiding carbon formation through the Boudouard reaction.[31,34] In addition, the operating conditions used in this work belong to the coke-free regime, according to Da Silva and Muller.[14] Higher amounts of methane were detected in the case of HM1 and HM2, thus suggesting CO methanation. However, CH_4 formation is not desired and a catalyst with high WGS activity is preferential to reduce the CO content of the product. In the liquid product, small amounts of acetaldehyde and acetic acid were detected for the cases of HM1 and HM2. This suggests that glycerol undergoes dehydration and subsequent dehydrogenation to form acetaldehyde, which is further converted to acetic acid.[45] At $T>673$ K, acetic acid may decompose over HM1 and HM2 to form CH_4 and CO_2. In the case of the Pt-promoted hybrid materials, no liquid

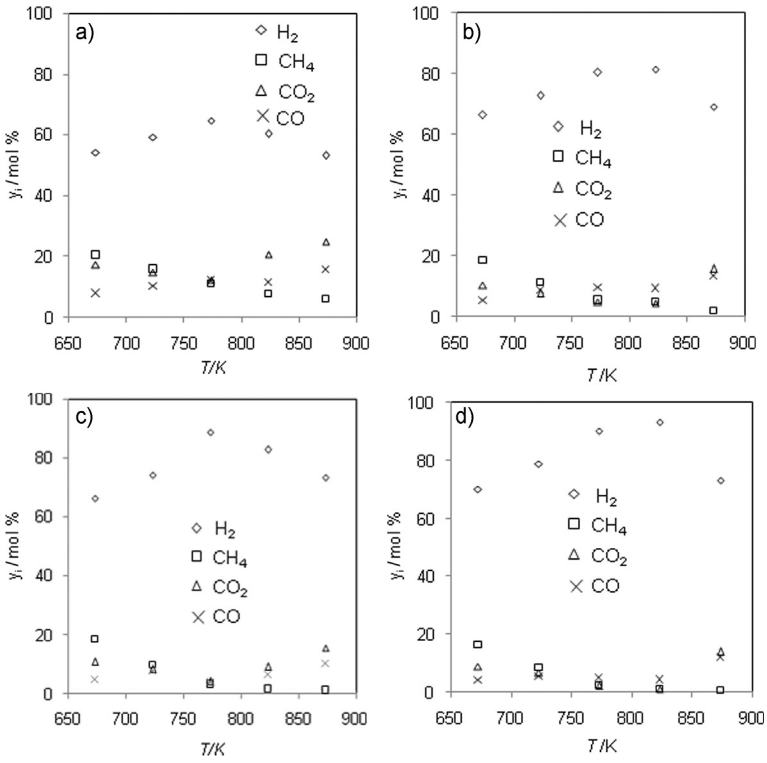

Figure 4. Product gas distribution (mol %) on a dry basis as a function of reaction temperature under steady-state conditions for the hybrid materials a) HM1, b) HM2, c) Pt-HM1, d) Pt-HM2. Reaction conditions: $P = 0.1$ MPa, GHSV = 3600 mL $g^{-1} h^{-1}$.

products were detected thus suggesting the complete decomposition of glycerol through C–C bond cleavage to form syngas. Thus, the addition of Pt as promoter to the hybrid materials improves H_2 production and avoids the formation of intermediates. The various reactions that occur in the system are:

$$\text{Glycerol decomposition}: \quad C_3H_8O_3 \rightarrow 3\,CO + 4\,H_2 \tag{1}$$

$$\text{Methanation reaction}: \quad CO + 3\,H_2 \rightarrow 3\,CH_4 + H_2O \tag{2}$$

$$\text{Water}-\text{gas shift}: \quad CO + H_2O \rightarrow H_2 + CO_2 \tag{3}$$

$$\text{Steam methane reforming}: \quad CH_4 + H_2O \rightarrow CO + 3\,H_2 \tag{4}$$

$$\text{Overall SESRG}: \quad C_3H_8O_3 + 3\,H_2O \rightarrow 3\,CO_2 + 7\,H_2 \tag{5}$$

SESRG studies

Breakthrough studies were performed to gain insights into the SESRG process. The dependency of concentrations of H_2 and CO_2 on time at $T = 773$ K and S/C = 9 mol mol^{-1} was studied. The results are represented in Figure 5.

Figure 5 a–d shows the breakthrough curves for the hybrid materials. Sorbent behavior is represented by breakthrough time (t_b) and adsorption capacity (Q_{ads}). The surface area and the presence of specific cations in the hybrid material influence the adsorption capacities. Three separate regions are evident, that is, pre-breakthrough, breakthrough, and post-breakthrough. In the pre-breakthrough stage, the adsorbent sites are readily available for adsorption. CO_2 formed during the steam reforming and WGS reactions is effectively adsorbed on the surface sites, thereby resulting in enhanced H_2 production. The highest concentrations of H_2 are seen in this region owing to the shift in the equilibrium. As time progresses, a gradual transition into the breakthrough stage occurs. In this region, the number of sites available for adsorption decreases, thus resulting in the increase in CO_2 levels. The breakthrough time of the adsorbent (t_b) is reached when CO_2 is detected in the outlet stream for the first time. As evident from Figure 5 c, d, both the Pt-promoted hybrid materials displayed longer breakthrough times (60 min and 75 min). This performance was superior to that reported in previous works.[27,34] Finally, as the sorbent gets completely saturated, no further adsorption takes place. In this post-breakthrough stage, the products reach their equilibrium values and the system exhibits a catalyst-only type behavior.

The efficacy of the hybrid materials can be evaluated in terms of the adsorption capacity, which was in the order Pt-HM2 > Pt-HM1 > HM2 > HM1 (see Table 3). The results obtained clearly suggest that Cu-based hybrid materials exhibit superior adsorption characteristics and produce high amounts of H_2. In particular, Pt-HM2 gave the highest adsorption capacity of 1.1 mol CO_2/kg sorbent in comparison to Pt-HM1 (0.84 mol CO_2/kg sorbent). These adsorption capacities are higher than those reported in our previous work.[27] Hybrid materials retain their sorption capacity until the breakthrough time (see Table 3). After that, this capacity is reduced. The CO_2 productivity of Pt-HM1 and Pt-HM2 was 0.016 and

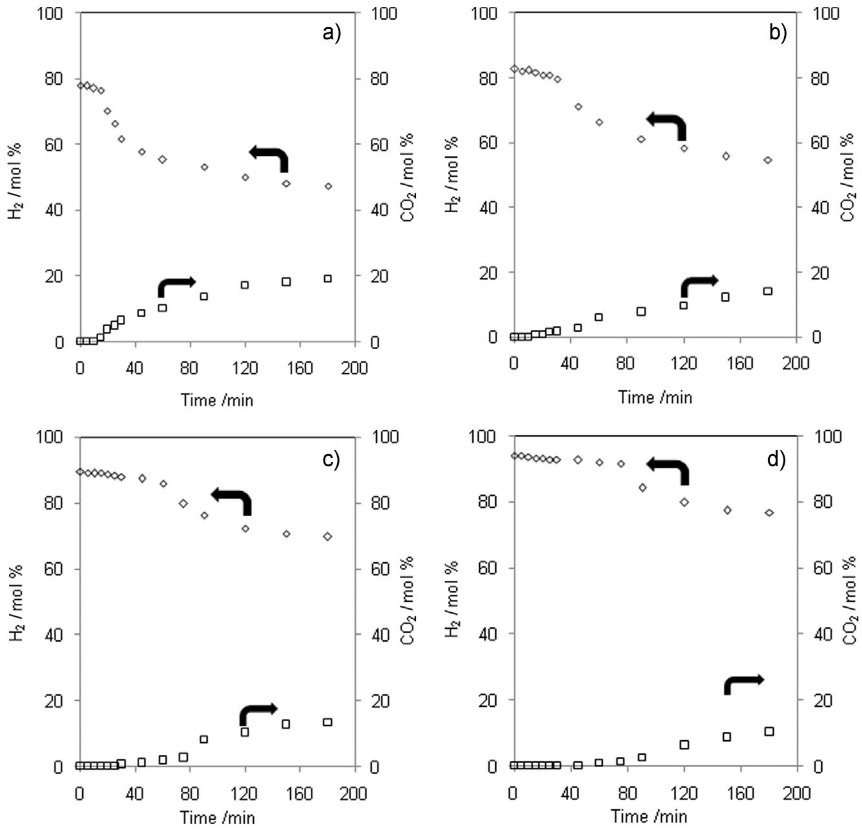

Figure 5. Breakthrough curves for hybrid materials a) HM1, b) HM2, c) Pt-HM1, d) Pt-HM2. Reaction conditions: $P=0.1$ MPa, $T=773$ K, steam/carbon ratio $=9$ mol mol^{-1}, GHSV $=3600$ mL g^{-1} h^{-1}, time on stream $=3$ h.

Table 3. Adsorption capacities of hybrid materials.[a]

Hybrid material	Breakthrough time (t_b) [min]	Q_{ads} [mol CO$_2$ kg$^{-1}_{sorbent}$]
HM1	15	0.36
HM2	30	0.52
Pt-HM1	60	0.84
Pt-HM2	75	1.1

[a] $P=0.1$ MPa, $T=773$ K, S/C ratio $=9$ mol mol^{-1}, GHSV $=3600$ mL g^{-1} h^{-1}, time on stream $=3$ h.

0.011 mol g^{-1} h^{-1}, respectively. The H_2 productivity of Pt-HM1 and Pt-HM2 was higher (0.13 and 0.16 mol g^{-1} h^{-1}) than that of HM1 and HM2 (0.07 and 0.09 mol g^{-1} h^{-1}). The enhancement in H_2 production and adsorption capacity can be attributed to the high surface area, which in turn leads to a higher number of adsorption sites for Pt-HM2. Also, the synergistic effect of the active metals (Pt, Ni, and Cu) along with the smaller crystal sizes resulted in higher activity and enhanced H_2 production. Both HM1 and HM2 showed lower adsorption capacities (0.36 and 0.52 mol CO_2/kg sorbent). This suggests that Pt addition to the hybrid materials results in improved H_2 production. Despite its low surface area, Pt-HM1 adsorbs more CO_2 than HM2, which is possibly due to its improved stability in the presence of Pt. Next, the influence of reaction variables on the performance of the Pt-promoted hybrid materials was studied.

Effect of temperature on SESRG

The effect of temperature on the performance of Pt-HM1 and Pt-HM2 was investigated in the range 673–873 K. The other reaction variables were chosen to be: $P=0.1$ MPa and S/C $=9$ mol mol^{-1}. At first, the H_2 concentration in the product stream increased with a rise in temperature, owing to the effective separation of CO_2 from the product (see Figure 6). The maximum value was reached at $T=773$ K (89.6 mol %) for Pt-HM1 and $T=823$ K (96 mol %) for Pt-HM2. After that, the H_2 concentration decreased with a further increase in temperature, which was possibly due to the inhibition of carbonation reactions.[27,46] Thus, the preferred operating temperatures for optimum H_2 production are 773 and 823 K for Pt-HM1 and Pt-HM2, respectively.

Effect of S/C ratio on SESRG

The S/C ratio is a crucial parameter that influences the economics of SESRG. The role of a high S/C ratio in diminishing carbon formation is renowned; however, the excess use of steam results in increased operating costs. Thus, developing hybrid materials that resist coking even at low values of S/C appears preferential. The influence of this parameter was investigated in the range 3–7.5 mol mol^{-1} at $T=773$ K (for Pt-HM1) and $T=823$ K (for Pt-HM2). The other parameter values were: $P=0.1$ MPa and GHSV $=3600$ mL g^{-1} h^{-1}. The increase in S/C

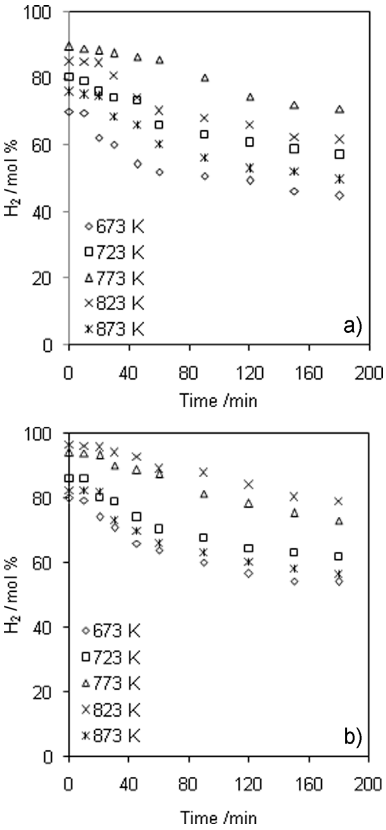

Figure 6. Effect of temperature on SER for hybrid materials a) Pt-HM1, b) Pt-HM2. Reaction conditions: $P=0.1$ MPa, steam/carbon ratio = 9 mol mol^{-1}, GHSV = 3600 mL g^{-1} h^{-1}, time on stream = 3 h.

ratio resulted in increased H_2 concentration in the product gas. The highest H_2 purity was 96.4 mol% H_2 (S/C = 6 mol mol^{-1}) for Pt-HM1 and 98.7 mol% H_2 (S/C = 4.5 mol mol^{-1}) for Pt-HM2. These results are represented in Figure 7 a, b. Notably, H_2 production decreased at higher S/C ratios for both materials. Such behavior is ascribed to the reduced CO_2 partial pressure at high values of S/C, thus resulting in reduced adsorption capacity.[30] Even so, it can be concluded that the Pt-promoted hybrid materials are efficient for H_2 production at lower S/C ratios.

Effect of sorbent mass fraction on SESRG

Knowledge of the optimum sorbent mass fraction for SESRG is essential. Both adsorption capacity and H_2 yield are dependent on the mass of hybrid material. The effect of sorbent mass fraction on H_2 yield was investigated in the range 0.09–0.27 kg h mol^{-1} at $P=0.1$ MPa. Pt-HM1 was tested at 773 K (S/C = 6 mol mol^{-1}) whereas Pt-HM2 was studied at 823 K (S/C = 4.5 mol mol^{-1}). As shown in Figure 8, the highest H_2 productivity was obtained at 0.27 kg h mol^{-1}. This corresponds to 3 g of hybrid material inside the reactor. This behavior is in line with previous works.[27,30]

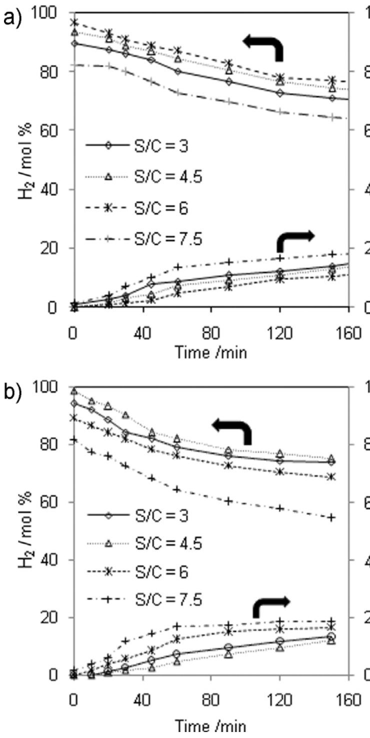

Figure 7. Effect of S/C ratios on SER for hybrid materials a) Pt-HM1, b) Pt-HM2. Reaction conditions: $P=0.1$ MPa, $T=773$ K (Pt-HM1) or 823 K (Pt-HM2), GHSV = 3600 mL g^{-1} h^{-1}, time on stream = 2.5 h.

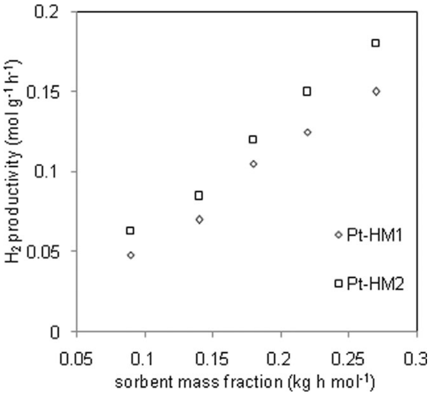

Figure 8. Effect of sorbent mass fraction on SESRG for hybrid materials. Reaction conditions: $P=0.1$ MPa, $T=773$ K (Pt-HM1) or 823 K (Pt-HM2), steam/carbon ratio = 6 mol mol^{-1} (for Pt-HM1) and 4.5 mol mol^{-1} (for Pt-HM2), time on stream = 2.5 h.

Cyclic stability tests

The development of highly stable sorbents is a prerequisite for the successful applications of SESRG. Sorbents that display multi-cycle durability and ease of regeneration are desirable. In previous work,[26] we showed that HTlc-like hybrid materials can be more easily regenerated than Ca-based materials. Treatment with excess steam at the reaction temperature is a straightforward method for the regeneration of HTlc-like hybrid materials.[27,47] The addition of steam regenerates the basic HTlc structure and also inhibits coke deposition.[47] To investigate the cyclic stability of the hybrid materials, 20 cycles of reaction and regeneration were performed. The reactions were carried out at the optimal conditions for the hybrid materials. In the case of our hybrid materials, the regeneration was carried out by passing excess steam (1.5 to 2 times the required flow rate of steam) at the reaction temperature for 20 min. The complete regeneration of CO_2 was ascertained by its presence in the exit stream from GC analysis.

The concentrations of H_2 and CO_2 over 20 cycles are reported (see Figure 9a–d). It is evident that both the Pt-promoted hybrid materials exhibit superior stability of up to 13 (Pt-HM1) and 18 (Pt-HM2) cycles. Contrarily, the un-promoted hybrid materials remained stable for five (HM1) and eight (HM2) cycles, respectively. The resilience and ease of regeneration of our materials make them suitable for real applications. The multi-cycle durability can be attributed to a strong metal–support interaction, improved CO_2 adsorption, and enhanced stability as a result of the presence of Pt. As evident from XRD analysis (Figure 10), the HTlc structure was largely retained after the cyclic tests. The marginal rise in crystallite sizes (see Table 4) suggested that the sintering effect on the Ni and Cu particles in the promoted materials was lowered. This suggests the role of Pt as a textural promoter in enhancing stability. Low intensity peaks for $MgAl_2O_4$ were observed for HM1 and Pt-HM1. A phase transformation from alumina to boehmite (AlOOH) was seen for all hybrid materials after the cyclic tests. In addition, distinct peaks for Cu and CuO along with spinel $CuAl_2O_4$ were detected for HM2 and Pt-HM2. Reduced Pt^0 species with increased crystallite size were obtained for both promoted materials. Our results were in line with previous works.[30,35,48] The cyclic stability of our Pt-promoted hybrid materials was higher than those reported previously.[23]

Towards the end of 20 cycles, the hybrid materials showed a decrease in H_2 concentrations. This reduction in H_2 production can be attributed to the sharp decline in the surface area (see Table 2). A plausible reason for the decrease in surface area may be metal sintering (see Table 4) and reduced porosity. The SEM images of the hybrid materials after 20 cyclic tests are shown in Figure 11a–d. It is noteworthy that our lab-made hybrid materials displayed encouraging performance in continuous operation cycles.

Reaction pathway

A schematic representation depicting the plausible SESRG reaction pathway over the investigated hybrid materials is proposed (see Figure 12).

The un-promoted hybrid materials HM1 and HM2 are assumed to follow the first pathway. In this route, the adsorbed glycerol molecule undergoes subsequent dehydration and dehydrogenation reactions. This leads to the formation of acetaldehyde. Then, the adsorbed acetaldehyde undergoes reactions of hydration–dehydrogenation to form acetic acid. This may be due to the fact that the hybrid material with basic features promotes fast dehydrogenation.[30] Acetic acid undergoes possible C–C bond cleavage to form CH_4, CO, CO_2, and H_2. The presence of Ni as an active agent effectively promotes C–C

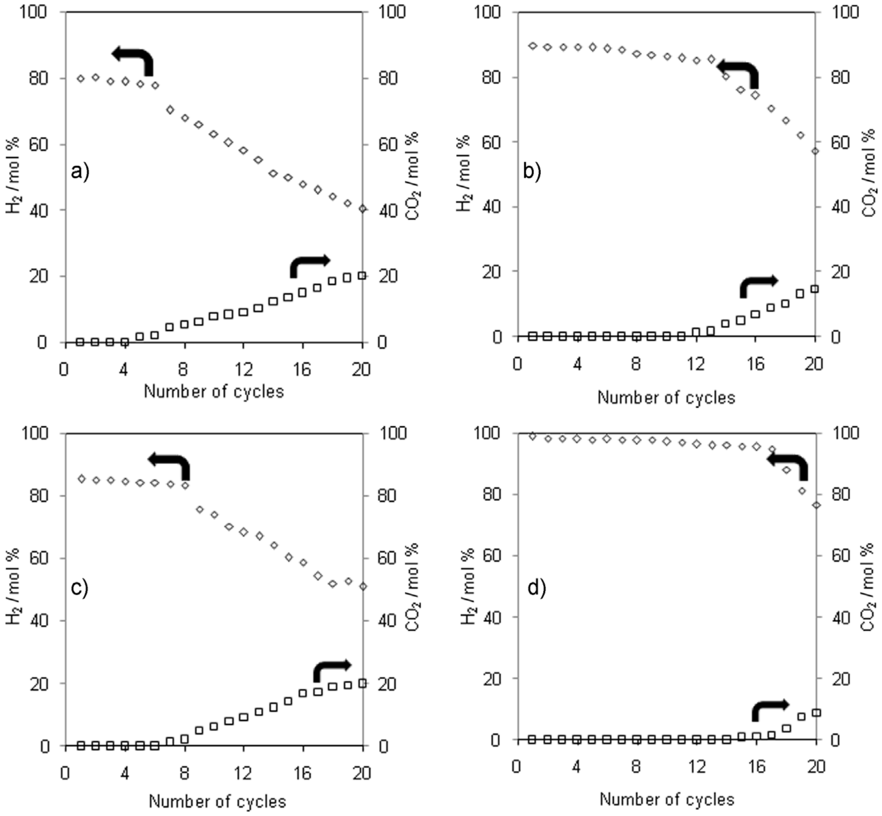

Figure 9. Cyclic stability studies for hybrid materials a) HM1, b) Pt-HM1, c) HM2, d) Pt-HM2. Reaction conditions: $P=0.1$ MPa, $T=773$ K (HM1 and Pt-HM1) or 823 K (HM2 and Pt-HM2), steam/carbon ratio $=6$ mol mol^{-1} (HM1 and Pt-HM1) or 4.5 mol mol^{-1} (HM2 and Pt-HM2), GHSV $=3600$ mL g^{-1} h^{-1}.

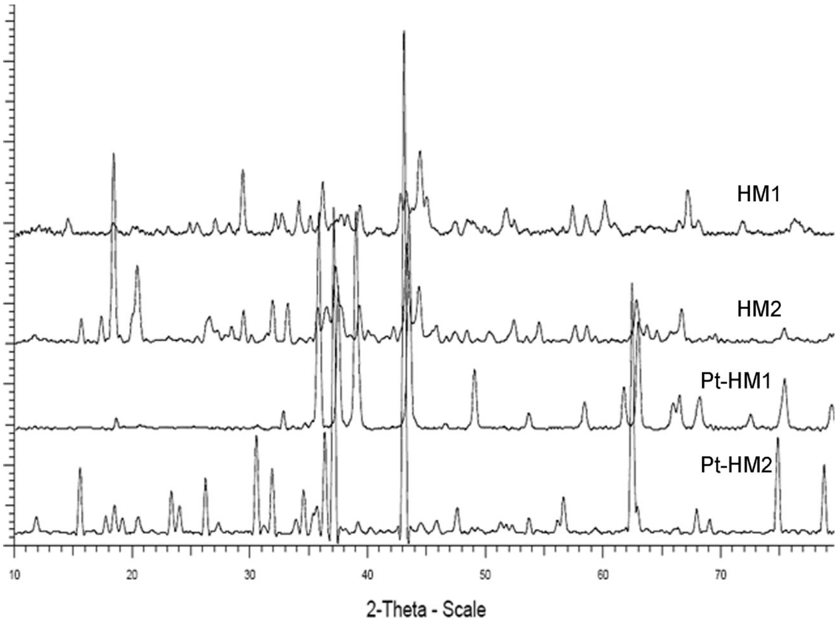

Figure 10. XRD patterns for the hybrid materials post cyclic tests.

Table 4. Crystallite sizes and phases of hybrid materials after cyclic tests.

Hybrid material	Phase	2θ position [°]	Crystallite size (d) [nm]
HM1	Ni	43.2	52.6
		53.5	20.6
	HTlc	37.3	48.5
	AlOOH	14.4	72.9
		28.1	43.8
		38.2	40.4
	$MgAl_2O_4$	36.1	39
		44.4	32
HM2	Ni	43.3	33.7
	AlOOH	28.4	65.9
		37.2	45.5
	Cu	52.4	27.5
		75.4	26.6
	CuO	35.7	54.4
		48.4	33.4
	$CuAl_2O_4$	63	24.4
Pt-HM1	Ni	43.5	34.7
		53.7	26.3
	HTc	37.5	41.3
	AlOOH	61.8	27.7
		75.5	18.9
	$MgAl_2O_4$	32.8	52.6
		66.5	15.1
	Pt^0	39	34.8
		68.2	17.2
Pt-HM2	Ni	43.1	36.7
	AlOOH	37.1	41.7
		78.8	24.6
	Cu	56.6	27.2
		74.9	25.1
	CuO	35.6	24
		36.3	45
	$CuAl_2O_4$	62.5	26.6
	Pt^0	47.6	30.1
		68	25.4

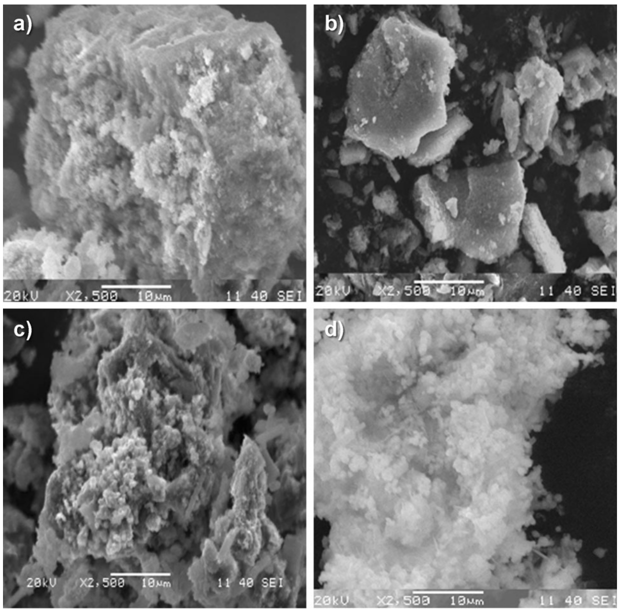

Figure 11. SEM images of hybrid materials after 20 cyclic tests: a) HM1, b) HM2, c) Pt-HM1, d) Pt-HM2.

bond rupture.[36] The products CO and CH_4 subsequently undergo WGS [Eq. (3)] and steam reforming [Eq. (4)] reactions to form CO_2 and H_2. In the case of HM1, there is a possibility for methanation of CO [Eq. (2)], leading to higher amounts of CH_4 being formed. Finally, the CO_2 formed gets adsorbed and pure H_2 is released.

For the case of the Pt-promoted hybrid materials, the second pathway seems feasible. In this pathway, fast decomposition involving C–C bond rupture of glycerol occurs

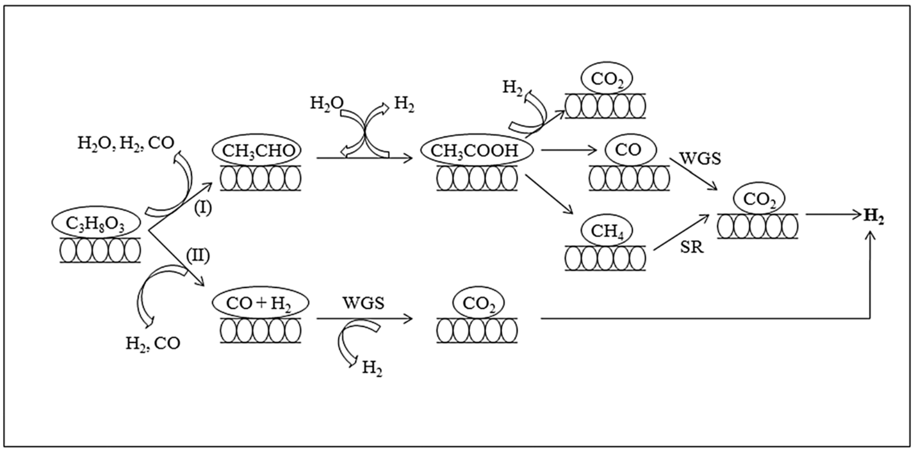

Figure 12. Proposed reaction pathways for SESRG.

[Eq. (1)]. This leads to the formation of syngas, which can be confirmed by the absence of liquid byproducts. Such absence of liquid intermediates in the SER of glycerol is not uncommon.[21] The adsorbed CO molecule then undergoes a WGS reaction to form CO_2 and H_2. The role of Ni, Mg, and Cu in the promotion of dehydrogenation reactions and C–C bond cleavage is renowned. In addition, the presence of Pt, which has high WGS activity and enhanced stability, is beneficial. As no significant intermediate byproducts are present, high concentrations of H_2 are obtained. In the end, the CO_2 thus formed gets effectively adsorbed, releasing H_2 in a way similar to the previous pathway. In conclusion, the hybrid material design plays a critical role in the formation of different products involved in the SESRG process.

General Remarks

Enhanced H_2 production along with satisfactory multi-cycle performance was achieved by using our Pt-promoted hybrid materials. From the optimization studies, we can determine the maximum adsorption capacities for the hybrid materials. Pt-HM1 gives a maximum adsorption capacity of 1.12 mol CO_2/kg sorbent at its optimal conditions, that is, $T = 773$ K, $P = 0.1$ MPa, S/C = 6 mol mol^{-1}, $t_b = 70$ min. The breakthrough time and adsorption capacity for Pt-HM1 was higher than that reported in previous works.[27,47] Importantly, Pt-HM2 exhibited the highest adsorption capacity of 1.34 mol CO_2/kg sorbent at its optimal conditions, that is, $T = 823$ K, $P = 0.1$ MPa, S/C = 4.5 mol mol^{-1}, $t_b = 90$ min. This adsorption capacity was much higher in comparison to an earlier work.[32] The adsorption capacities of the Pt-promoted materials were much superior to those for the un-promoted materials. HM1 and HM2 gave adsorption capacities of 0.65 and 0.9 mol CO_2/kg sorbent, respectively. The addition of a noble metal such as Pt to the hybrid materials proved successful for enhancing the adsorption capacity. However, there is scope for improving the multi-cycle performance by modifying the anions or addition of suitable metals to the HTlc structure.

Conclusions

Pt-promoted cationic-modified HTlc-based hybrid materials were investigated for effective in situ CO_2 removal and improved H_2 production. Both the Pt-promoted hybrid materials possessed higher adsorption capacities and cyclic stability in comparison to the un-promoted materials. Optimization of the SESRG process was done by evaluating the effect of various reaction variables on the performance of the Pt-promoted hybrid materials. Amongst all the hybrid materials, Pt-HM2 showed great potential for enhanced H_2 production. It gave the highest H_2 concentrations (above 98 mol %) and adsorption capacities (1.34 mol CO_2/kg sorbent) at its optimal conditions. A reaction pathway demonstrating the role of the various metals in the hybrid materials was suggested. Such novel multi-functional materials are promising for improved H_2 production.

Experimental Section

Materials

Nickel nitrate, magnesium nitrate, copper nitrate, aluminium nitrate, sodium carbonate, sodium hydroxide, and chloroplatinic acid hexahydrate used in the synthesis of the HTlc-based hybrid materials were procured from Sigma–Aldrich Pvt. Ltd., Mumbai. Glycerol (purity 99 %), used in all experiments, was also purchased from Sigma–Aldrich Pvt. Ltd., Mumbai. Gases such as air, H_2, and nitrogen (N_2) in cylinders (purity 99.995 %) were acquired from Industrial Oxygen Company Ltd., Mumbai. Standard calibration gas mixtures containing CO, CO_2, and CH_4 were procured from Chemtron Laboratory Pvt. Ltd, Mumbai.

Hybrid material synthesis

A co-precipitation technique was used to synthesize the HTlc hybrid materials (NiMgHTlc and NiCuHTlc) according to a method previously reported in the literature.[49] Nitrates of the respective aforesaid metal components were used in appropriate amounts. The ratio of M^{2+}/M^{3+} was selected as 3 so as to have a higher basicity in the material, thereby leading to effective adsorption of

CO_2. An aqueous solution of the metal nitrates was slowly added into a beaker containing an aqueous solution of sodium carbonate under continuous stirring at room temperature and constant pH of 10. The pH of the solution was maintained by using an aqueous solution of sodium hydroxide (2 M). The resulting suspension was then kept at room temperature for 24 h. The precipitate thus obtained was filtered and washed several times with de-ionized water to remove any traces of nitrates; this was further confirmed by the brown ring test. The resulting material was dried at 383 K overnight and ground into a fine powder and calcined at 1073 K for 5 h in air. The addition of platinum (2.5 wt%) to the prepared hybrid materials was carried out by the incipient wetness impregnation technique. An aqueous solution of chloroplatinic acid hexahydrate was impregnated over the HTlc material. The resulting material was dried at 383 K for 2 h and calcined at 873 K for 4 h. The material was then crushed and sieved to fine particles with 30–60 mesh size (0.3–0.6 mm). In all the hybrid materials, 10 wt% nickel loading was maintained. The hybrid materials were designated as NiMgHTlc (HM1), Pt-NiMgHTlc (Pt-HM1), NiCuHTlc (HM2), and Pt-NiCuHTlc (Pt-HM2).

Characterization of hybrid materials

The synthesized hybrid materials were characterized by using several physico-chemical techniques. Crystallinity and textural patterns were predicted from XRD (X-ray diffraction) data, which were recorded by using a Rigaku–miniflex powder diffractometer with CuK (1.54 Å) radiation. Nitrogen adsorption–desorption techniques (Micromeritics ASAP2010) were used to find the BET (Brunauer–Emmet–Teller) surface area, pore volume, and pore diameter by BJH (Barrett–Joyner–Halenda) and multipoint BET method. SEM (scanning electron microscope) micrographs and EDX (energy dispersive X-ray spectroscopy) data were obtained by using a JEOL-JSM 6380 LA instrument.

Experimental setup

A SS-316 tubular fixed-bed down-flow reactor (inner diameter 19 mm, outer diameter 25.4 mm, and length 560 mm), purchased from Chemito Technologies Pvt. Ltd., Mumbai, was used in all experiments. The setup was supplied with a control panel, temperature-controlled furnace, gas chromatograph (GC 8610) unit, and a data acquisition system (Proficy HMI/SCADA-ifax software). The temperature was controlled by using a temperature controller (West, Germany). A pressure transducer (0–100 bar) enabled the measurement of pressure with an uncertainty of ±0.1 bar.

Experimental procedure

In all experiments, the hybrid material was packed within a thin bed of quartz wool. The catalyst was reduced inside the reactor under flowing H_2 (10 L h^{-1}) for 1 h. An aqueous solution of glycerol was pumped at the chosen flow rate from a feed vessel by using an HPLC pump. N_2 was used as the carrier gas during the reaction. The N_2 flow rate was adjusted to the desired value with an accuracy of ±1 cm^3 min^{-1}. The water/glycerol mixture was vaporized in a pre-heater and passed through the reactor at the desired temperature. The pre-heater temperature was maintained at 523 K. All experiments were performed at ambient pressure. The product vapors leaving the reactor were passed through a condenser, back-pressure regulator, and gas-liquid separator. Product gases were analyzed online by using a gas chromatograph (GC) unit equipped with a TCD. A Hayesep DB column (length 3.6 m) was used for detecting H_2, CH_4, CO_2, and CO. In addition, the liquid products were periodically collected and analyzed by GC employing Tenax column (length 1.9 m). Standard calibration gas and liquid mixtures were used to determine the product composition. The steam-to-carbon ratio was equal to 9 mol mol^{-1} unless stated otherwise. The liquid feed rate was varied from 0.25 to 1.25 mL min^{-1}.

The conversion of glycerol was defined as follows:

$$\text{Glycerol conversion}\,(\%) = \frac{[\text{Glycerol}]_{\text{in}} - [\text{Glycerol}]_{\text{out}}}{[\text{Glycerol}]_{\text{in}}} \times 100 \tag{6}$$

where $[\text{Glycerol}]_{\text{in}}$ and $[\text{Glycerol}]_{\text{out}}$ represent the inlet and outlet molar flow rate (mol h^{-1}) of glycerol. The H_2 yield was defined as:

$$H_2\,\text{yield}\,(\%) = \frac{[H_2]_{\text{out}}}{7 \times [\text{Glycerol}]_{\text{in}}} \times 100 \tag{7}$$

where $[H_2]_{\text{out}}$ represents the outlet molar flow rate (mol h^{-1}) of H_2. The gas hourly space velocity (GHSV) was defined as:

$$\text{GHSV} = \text{Inlet gas flow}\,(\text{mL min}^{-1})/\text{Weight of material}\,(\text{g}) \tag{8}$$

The adsorption capacity of the adsorbents was calculated by using the relationship:

$$Q_{\text{ads}} = \frac{[F \times C_0 \times t_b]}{W} \tag{9}$$

where F is the total molar flow of the feed gas (mol min^{-1}), C_0 is the initial CO_2 concentration (mole %), W is the mass of the solid adsorbent loaded on the column (g), and t_b is the stoichiometric time in minutes, determined from the breakthrough curve.

Acknowledgments

K.D.D. is thankful to the Department of Science and Technology, Government of India, New Delhi, for providing financial assistance (DST-INSPIRE [IF140201]). P.D.V. is grateful to the Technical Education Quality Improvement Program (TEQIP) Phase II—Center of Excellence for Process Intensification (CoEPI) at ICT, Mumbai.

Keywords: glycerol · hydrogen · sorption-enhanced reforming

[1] P. D. Vaidya, A. E. Rodrigues, *Chem. Eng. Technol.* **2009**, *32*, 1463–1469.
[2] S. Adhikari, S. D. Fernando, A. Haryanto, *Energy Convers. Manage.* **2009**, *50*, 2600–2604.
[3] S. Adhikari, S. Fernando, A. Haryanto, *Catal. Today* **2007**, *129*, 355–364.
[4] T. Montini, R. Singh, P. Das, B. Lorenzut, N. Bertero, P. Riello, A. Benedetti, G. Giambastiani, C. Bianchini, S. Zinoviev, S. Miertus, P. Fornasiero, *ChemSusChem* **2010**, *3*, 619–628.
[5] A. Iriondo, V. L. Barrio, J. F. Cambra, P. L. Arias, M. B. Güemez, R. M. Navarro, M. C. Sánchez-Sánchez, J. L. G. Fierro, *Catal. Commun.* **2009**, *10*, 1275–1278.
[6] V. Chiodo, S. Freni, A. Galvagno, N. Mondello, F. Frusteri, *Appl. Catal. A* **2010**, *381*, 1–7.
[7] B. Zhang, X. Tang, Y. Li, Y. Xu, W. Shen, *Int. J. Hydrogen Energy* **2007**, *32*, 2367–2373.
[8] R. R. Soares, D. A. Simonetti, J. A. Dumesic, *Angew. Chem. Int. Ed.* **2006**, *45*, 3982–3985; *Angew. Chem.* **2006**, *118*, 4086–4089.

[9] M. Shokrollahi Yancheshmeh, H. R. Radfarnia, M. C. Iliuta, *Chem. Eng. J.* **2016**, *283*, 420–444.
[10] J. Fermoso, L. He, D. Chen, *J. Chem. Technol. Biotechnol.* **2012**, *87*, 1367–1374.
[11] B. Dou, Y. Song, C. Wang, H. Chen, Y. Xu, *Renewable Sustainable Energy Rev.* **2014**, *30*, 950–960.
[12] R. Wess, F. Nores-Pondal, M. Laborde, P. Giunta, *Chem. Eng. Sci.* **2015**, *134*, 86–95.
[13] J. M. Silva, M. A. Soria, L. M. Madeira, *J. Power Sources* **2015**, *273*, 423–430.
[14] A. Lima da Silva, I. A. Müller, *Int. J. Hydrogen Energy* **2011**, *36*, 2057–2075.
[15] I. Iliuta, H. R. Radfarnia, M. C. Iliuta, *AIChE J.* **2013**, *59*, 2105–2118.
[16] J. M. Silva, M. A. Soria, L. M. Madeira, *Renewable Sustainable Energy Rev.* **2015**, *42*, 1187–1213.
[17] N. Sánchez, J. M. Encinar, J. F. González, *Ind. Eng. Chem. Res.* **2016**, *55*, 3736–3741.
[18] B. Dou, B. Jiang, Y. Song, C. Zhang, C. Wang, H. Chen, B. Du, Y. Xu, *Fuel* **2016**, *166*, 340–346.
[19] B. Dou, C. Wang, H. Chen, Y. Song, B. Xie, *Int. J. Hydrogen Energy* **2013**, *38*, 11902–11909.
[20] B. Dou, V. Dupont, G. Rickett, N. Blakeman, P. T. Williams, H. Chen, Y. Ding, M. Ghadiri, *Bioresour. Technol.* **2009**, *100*, 3540–3547.
[21] C. Wang, Y. Chen, Z. Cheng, X. Luo, L. Jia, M. Song, B. Jiang, B. Dou, *Energy Fuels* **2015**, *29*, 7408–7418.
[22] L. He, J. M. S. Parra, E. A. Blekkan, D. Chen, *Energy Environ. Sci.* **2010**, *3*, 1046–1056.
[23] J. Fermoso, L. He, D. Chen, *Int. J. Hydrogen Energy* **2012**, *37*, 14047–14054.
[24] C. Dang, H. Yu, H. Wang, F. Peng, Y. Yang, *Chem. Eng. J.* **2016**, *286*, 329–338.
[25] C. Wang, B. Dou, B. Jiang, Y. Song, B. Du, C. Zhang, K. Wang, H. Chen, Y. Xu, *Int. J. Hydrogen Energy* **2015**, *40*, 7037–7044.
[26] K. D. Dewoolkar, P. D. Vaidya, *Energy Fuels* **2015**, *29*, 3870–3878.
[27] K. D. Dewoolkar, P. D. Vaidya, *Int. J. Hydrogen Energy* **2016**, *41*, 6094–6106.
[28] S. M. De Rezende, C. A. Franchini, M. L. Dieuzeide, A. M. D. De Farias, N. Amadeo, M. A. Fraga, *Chem. Eng. J.* **2015**, *272*, 108–118.
[29] J. S. Valente, J. H. Cortez, M. S. Cantu, G. Ferrat, E. L. Salinas, *Catal. Today* **2010**, *150*, 340–345.
[30] Y. J. Wu, P. Li, J. G. Yu, A. F. Cunha, A. E. Rodrigues, *Chem. Eng. J.* **2013**, *231*, 36–48.
[31] T. Shishido, M. Yamamoto, I. Atake, D. L. Li, Y. Tian, H. Morioka, *J. Mol. Catal. A* **2006**, *253*, 270–278.
[32] A. F. Cunha, Y. J. Wu, J. C. Santos, A. E. Rodrigues, *Ind. Eng. Chem. Res.* **2012**, *51*, 13132–13143.
[33] C. Wang, B. Dou, H. Chen, Y. Song, Y. Xu, X. Du, T. Luo, C. Tan, *Chem. Eng. J.* **2013**, *220*, 133–142.
[34] C. Wang, B. Dou, H. Chen, Y. Song, Y. Xu, X. Du, L. Zhang, T. Luo, C. Tan, *Int. J. Hydrogen Energy* **2013**, *38*, 3562–3571.
[35] A. F. Cunha, Y. J. Wu, P. Li, J. G. Yu, A. E. Rodrigues, *Ind. Eng. Chem. Res.* **2014**, *53*, 3842–3853.
[36] P. D. Vaidya, A. E. Rodrigues, *Chem. Eng. J.* **2006**, *117*, 39–49.
[37] S. Narayanan, K. Krishna, *Catal. Today* **1999**, *49*, 57–63.
[38] H. J. Lee, Y. S. Lim, N. C. Park, Y. C. Kim, *Chem. Eng. J.* **2009**, *146*, 295–301.
[39] D. A. Boga, R. Oord, A. M. Beale, Y. M. Chung, P. C. A. Bruijnincx, B. M. Weckhuysen, *ChemCatChem* **2013**, *5*, 529–537.
[40] A. Aristizábal, S. Contreras, N. Barrabés, J. Llorca, D. Tichit, F. Medina, *Appl. Catal. B* **2011**, *110*, 58–70.
[41] A. F. Cunha, Y. J. Wu, J. C. Santos, A. E. Rodrigues, *Chem. Eng. Res. Des.* **2013**, *91*, 581–592.
[42] H. S. Chen, T. F. Zhang, B. L. Dou, V. Dupont, P. T. Williams, M. Ghadiri, Y. Ding, *Int. J. Hydrogen Energy* **2009**, *34*, 7208–7222.
[43] T. Hirai, N. O. Ikenaga, T. Miyake, T. Suzuki, *Energy Fuels* **2005**, *19*, 1761–1762.
[44] A. M. D. Douette, S. Q. Turn, W. Wang, W. I. Keffer, *Energy Fuels* **2007**, *21*, 3499–3504.
[45] F. Pompeo, G. Santori, N. N. Nichio, *Int. J. Hydrogen Energy* **2010**, *35*, 8912–8920.
[46] F. Cavani, F. Trifiro, A. Vaccari, *Catal. Today* **1991**, *11*, 173–301.
[47] P. Harrison, *Ind. Eng. Chem. Res.* **2008**, *47*, 6486–6501.
[48] M. García-Diéguez, E. Finocchio, M. Á. Larrubia, L. A. Alemany, G. Busca, *J. Catal.* **2010**, *274*, 11–20.
[49] D. Li, L. Wang, M. Koike, Y. Nakagawa, K. Tomishige, *Appl. Catal. B* **2011**, *102*, 528–538.

Received: June 30, 2016